# The impact of solid-solution composition on kinetics and mechanism of [2+2] photodimerizations of cinnamic acid derivatives.

Lorenzo Pandolfi,[a] Andrea Giunchi,[a] Tommaso Salzillo,*[ab] Aldo Brillante,[a] Raffaele G. Della Valle,[a] Elisabetta Venuti,*[a] Fabrizia Grepioni,[c] and Simone D'Agostino*[c]

[a] Dipartimento di Chimica Industriale "Toso Montanari", Università di Bologna, viale del Risorgimento, 4, 40136, Bologna.

[b] Department of Materials and interfaces, Weizmann Institute of Science, Herzl street 234, 76100 Rehovot, Israel.

[c] Dipartimento di Chimica "Giacomo Ciamician", Università di Bologna, Via Francesco Selmi, 2, 40126, Bologna, Italy.

| ***Table of Contents*** | |
|---|---|

**Table ESI-1.** Crystal data and details of measurements for crystalline [**1**H]$Br_xCl_{1-x}$ (x = 0.25, 0.50 and 0.75) before and after 2 h of irradiation (partial photoconversion), and of the photodimers [$\mathbf{1}_2H_2$]$Br_{0.5}Cl_{1.5}$, [$\mathbf{1}_2H_2$]BrCl, and [$\mathbf{1}_2H_2$]$Br_{1.5}Cl_{0.5}$.

| | [**1**H]$Br_{0.25}Cl_{0.75}$ | [**1**H]$Br_{0.25}Cl_{0.75}$_2h | [$\mathbf{1}_2H_2$]$Br_{0.5}Cl_{1.5}$ | [**1**H]$Br_{0.5}Cl_{0.5}$ | [**1**H]$Br_{0.5}Cl_{0.5}$_2h | [$\mathbf{1}_2H_2$]BrCl | [**1**H]$Br_{0.75}Cl_{0.25}$ | [**1**H]$Br_{0.75}Cl_{0.5}$_2h | [$\mathbf{1}_2H_2$]$Br_{1.5}Cl_{0.5}$ |
|---|---|---|---|---|---|---|---|---|---|
| Formula | $C_9H_{10}NO_2Br_{0.25}Cl_{0.75}$ | $C_9H_{10}NO_2Br_{0.25}Cl_{0.75}$ | $C_{18}H_{20}N_2O_4Br_{0.5}C_{.5}$ | $C_9H_{10}NO_2Br_{0.5}Cl_{0.5}$ | $C_9H_{10}NO_2Br_{0.5}Cl_{0.5}$ | $C_{18}H_{20}N_2O_4BrCl$ | $C_9H_{10}NO_2Br_{0.75}Cl_{0.25}$ | $C_9H_{10}NO_2Br_{0.75}Cl_{0.25}$ | $C_{18}H_{20}N_2O_4Br_{1.5}Cl_{0.5}$ |
| Formula weight | 210.74 | 210.74 | 421.48 | 221.86 | 221.86 | 443.72 | 232.97 | 232.97 | 465.94 |
| Cryst. System | Monoclinic | Monoclinic | Monoclinic | Monoclinic | Monoclinic | Monoclinic | Monoclinic | Monoclinic | Monoclinic |
| Space group | $P2_1/c$ | $P2_1/c$ | $P2_1/c$ | $P2_1/c$ | $P2_1/c$ | $P2_1/c$ | $P2_1/c$ | $P2_1/c$ | $P2_1/c$ |
| Z | 4 | 4 | 2 (Z'=0.5) | 4 | 4 | 2 (Z'=0.5) | 4 | 4 | 2 (Z'=0.5) |
| a (Å) | 5.6333(2) | 5.6612(4) | 5.8421(7) | 5.7177(2) | 5.8044(7) | 5.9100(4) | 5.7913(3) | 5.8290(16) | 5.9566(6) |
| b (Å) | 8.5840(4) | 8.6217(7) | 8.2764(14) | 8.6998(4) | 8.6743(12) | 8.6120(10) | 8.7920(6) | 8.757(2) | 8.7112(9) |
| c (Å) | 19.6694(9) | 19.164(2) | 18.838(3) | 19.4040(9) | 18.561(3) | 18.0253(16) | 19.0844(18) | 18.712(8) | 18.065(3) |
| α (deg) | 90 | 90 | 90 | 90 | 90 | 90 | 90 | 90 | 90 |
| β (deg) | 92.184(4) | 91.532(8) | 92.673(13) | 92.210(4) | 91.675(12) | 91.628(7) | 92.462(6) | 91.96(3) | 92.015(12) |
| γ (deg) | 90 | 90 | 90 | 90 | 90 | 90 | 90 | 90 | 90 |
| V (Å$^3$) | 950.44(7) | 935.03(14) | 909.9(2) | 964.49(7) | 934.1(2) | 917.06(15) | 970.83(12) | 954.6(5) | 936.8(2) |
| $D_{calc}$ (g/cm$^3$) | 1.473 | 1.497 | 1.546 | 1.5278 | 1.578 | 1.607 | 1.594 | 1.621 | 1.652 |
| μ (mm$^{-1}$) | 1.348 | 1.370 | 1.408 | 2.295 | 2.369 | 2.414 | 3.240 | 3.295 | 3.358 |
| Measured reflections | 4072 | 4235 | 3786 | 3954 | 7686 | 4168 | 4316 | 3994 | 4006 |
| Independent reflections | 2191 | 2135 | 2061 | 2187 | 2276 | 2116 | 2236 | 1678 | 2147 |
| $R_1$[on $F_0^2$, I>2σ(I)] | 0.0524 | 0.0580 | 0.0898 | 0.0552 | 0.0783 | 0.0692 | 0.0439 | 0.1319 | 0.0678 |
| $wR_2$ (all data) | 0.1396 | 0.1765 | 0.2608 | 0.122 | 0.1840 | 0.1339 | 0.0918 | 0.3464 | 0.1938 |

***Hydrogen bonds and distances d in [1H]Cl, [1H]$B_xCl_{1-x}$ (x = 0.25, 0.5, 0.75) and [1H]Br***

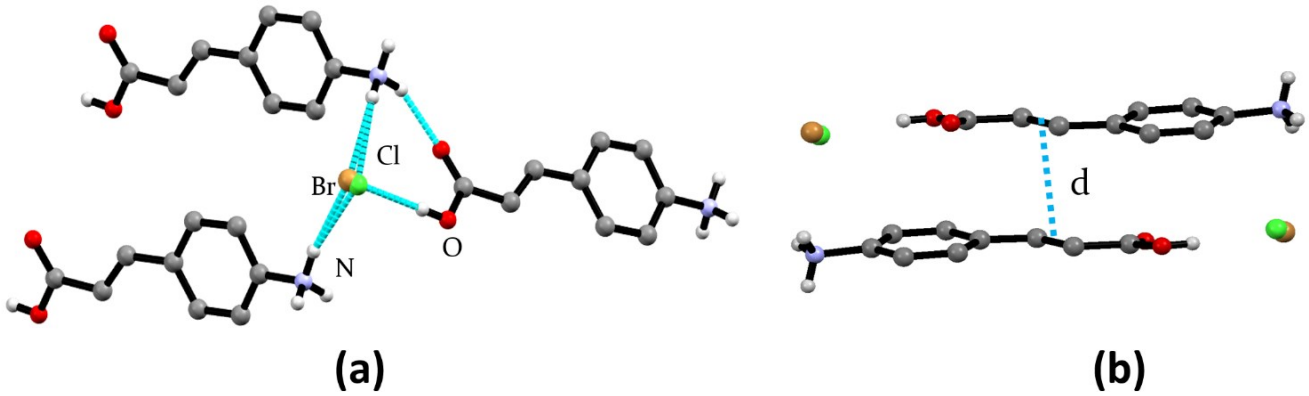


**Figure ESI-1.** Charge-assisted hydrogen bonding interactions detected within [**1**H]$Br_{0.5}Cl_{0.5}$.

**Table ESI-2.** Comparison between the charge-assisted hydrogen bonding interactions N-$H^+$···$X^-$ or O···$X^-$ and the centre-to-centre distance (**d**) between double-bonds (Schmidt's criterion) of the head-to-tail arrangements within [**1**H]Cl, [**1**H]$Br_xCl_{1-x}$ (0.25, 0.5, 0.75) and [**1**H]Br.

| | **N-$H^+$···$X^-$** | | **O···$X^-$(Å)** | | |
|---|---|---|---|---|---|
| **$x_{Br}$** | **N···$Br^-$ (Å)** | **N···$Cl^-$ (Å)** | **O···$Br^-$(Å)** | **O···$Cl^-$(Å)** | **d (Å)** |
| **0**[a] | - | 3.140(4)-3.194(4) | - | 3.056(3) | 3.657(5) |
| **0.25** | 3.148(4)-3.230(4) | 3.183(4)-3.240(4) | 3.259(4) | 3.009(4) | 3.643(5) |
| **0.5** | 3.200(3)-3.264(3) | 3.239(1)-3.393(3) | 3.235(3) | 3.028(3) | 3.637(5) |
| **0.75** | 3.252(3)-3.360(6) | 3.266(6)-3.360(6) | 3.211(3) | 3.222(6) | 3.622(4) |
| **1**[b] | 3.291(3)- 3.345(3) | - | 3.248(4) | - | 3.618(6) |

[a] = structural data from reference [1]; [b] = structural data from reference [2].

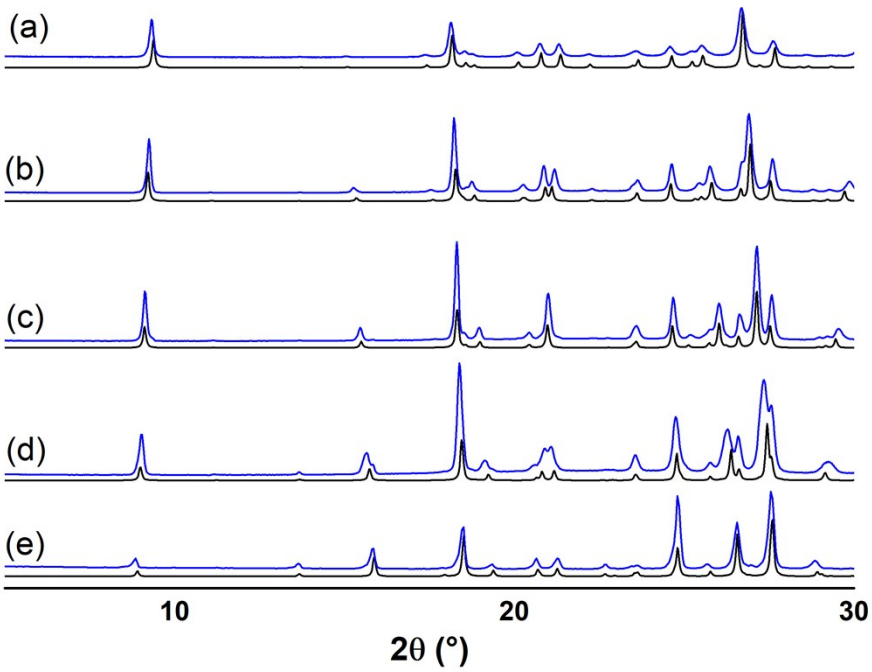


**Figure ESI-2.** Experimental (blue line) and simulated (black line) X-ray powder diffraction patterns of: (a) [**1**H]Br, (b) [**1**H]$Br_{0.75}Cl_{0.25}$, (c) [**1**H]$Br_{0.5}Cl_{0.5}$, (d) [**1**H]$Br_{0.25}Cl_{0.75}$ and (e) [**1**H]Cl.

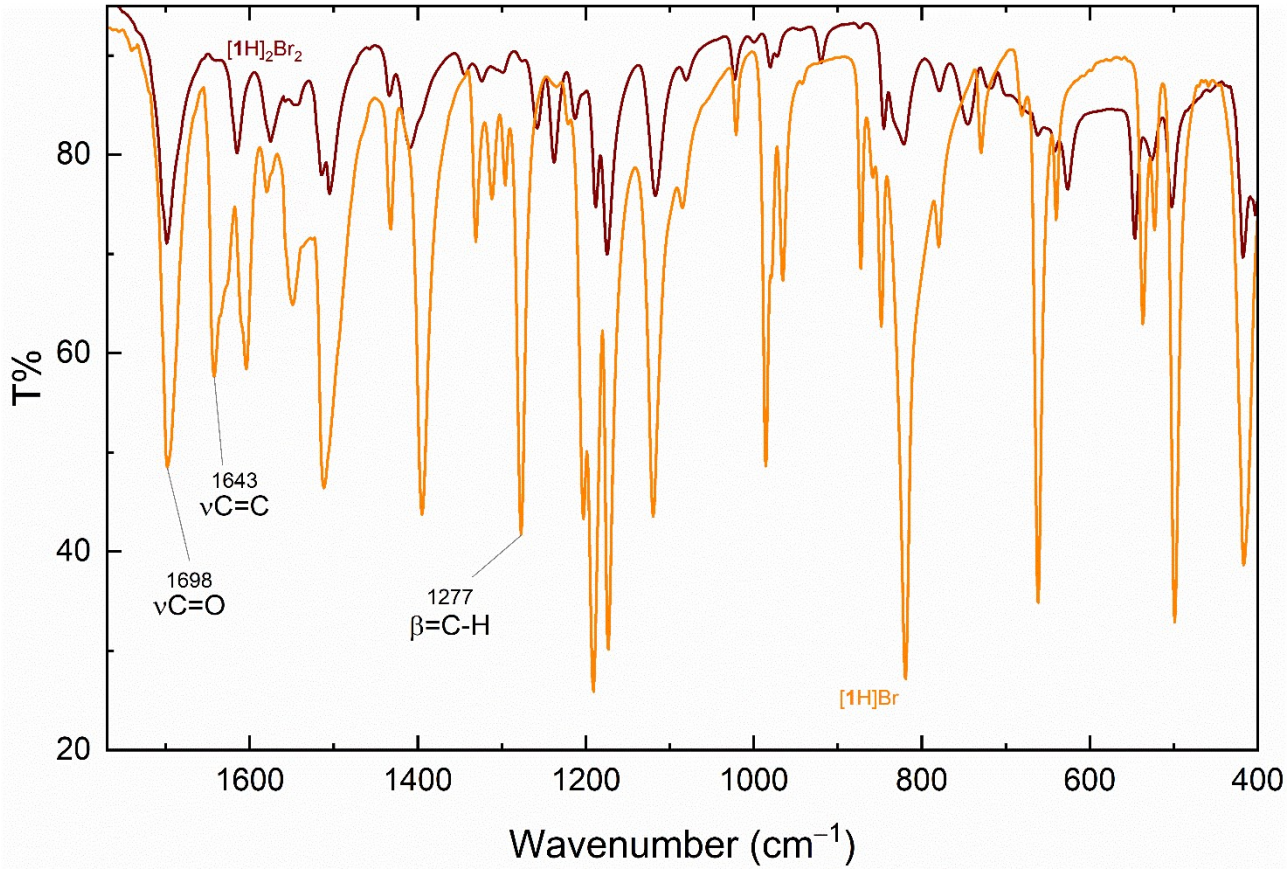


**Figure ESI-3.** FTIR-ATR spectra of the powders of the [**1**H]Br monomer at t = 0 (orange trace) and after prolonged irradiation at λ = 365 nm (brown trace), when no more changes were detected. In the spectrum of the monomer the bands diagnostic for the dimerization are indicated.

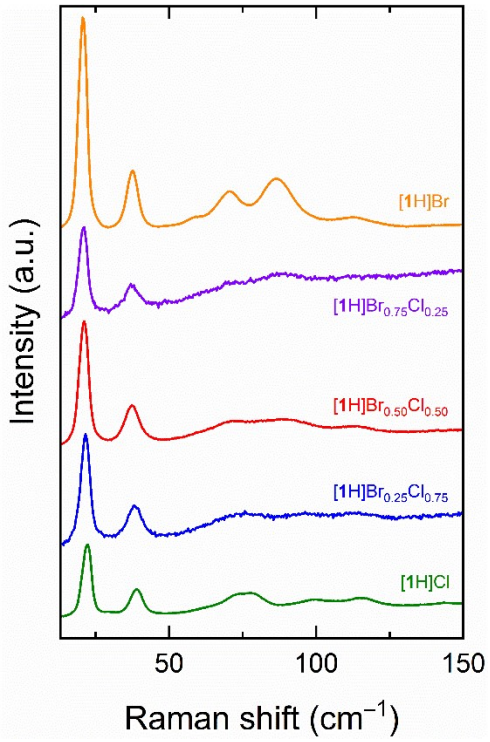


**Figure SI-4**. Raman spectra in the lattice phonon interval of single crystals of [**1**H]Br, [**1**H]$Br_{0.75}Cl_{0.25}$, [**1**H]$Br_{0.5}Cl_{0.5}$, [**1**H]$Br_{0.25}Cl_{0.75}$ and [**1**H]Cl (from top to bottom).

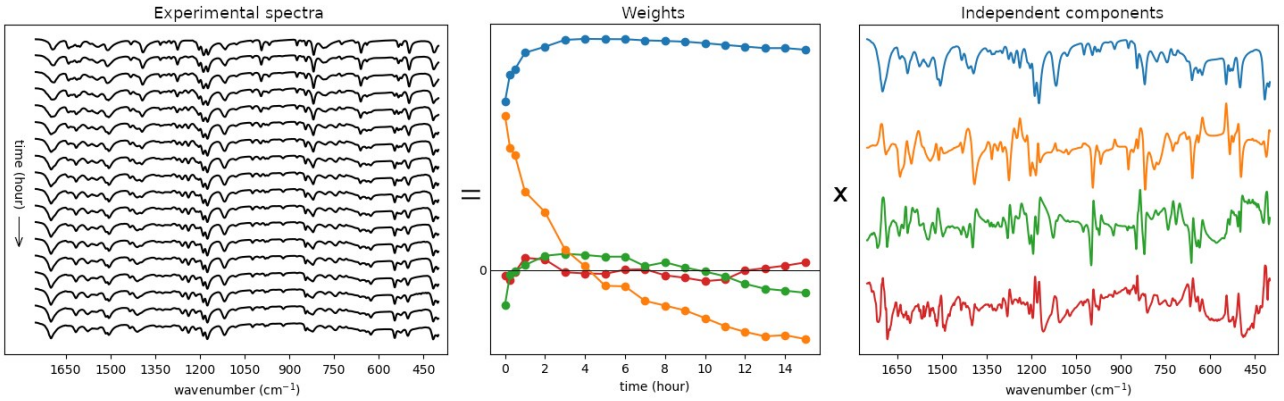


**Figure ESI-5.** PCA applied to FTIR-ATR spectra of [**1**H]Br collected during the progress of the reaction: spectra as a function of time after removing constant baselines and intensity fluctuations by normalization to zero mean and unit variance (left); independent components in which the spectra can be decomposed (right) and weights of such components (centre, drawn with matching colors). Only the first four components and the corresponding weights are shown. The weight $w_{PCA}(t)$ of the second component (orange) describes the progress of the reaction and has a linear relationship with the unreacted fraction $\alpha(t)$ of the monomer.

***The kinetic scheme***

The rate equations for the proposed kinetic scheme (Figure 6 of the main text) are the following:

$$\frac{d[M]}{dt} = -2k_1 I_v[M] + k_2[M^*] - k_3[M][M^*] + k_4[MM^*] \#(1)$$

$$\frac{d[M^*]}{dt} = 2k_1 I_v[M] - k_2[M^*] - k_3[M][M^*] + k_4[MM^*] \#(2)$$

$$\frac{d[MM^*]}{dt} = k_3[M][M^*] - k_4[MM^*] - k_5[MM^*] \#(3)$$

$$\frac{d[D]}{dt} = k_5[MM^*] \#(4)$$

Where $M$ and $M^*$ is the monomer in its ground and excited state, respectively; $MM^*$ is the excimer and $D$ is the dimer product.

By assuming steady state conditions $\frac{d[M^*]}{dt} = \frac{d[MM^*]}{dt} = 0$, we can solve the system of equations and obtain the concentrations of the intermediate species:

$$[MM^*] = \frac{k_3 I_v[M][M^*]}{k_4 + k_5} \#(5)$$

$$[M^*] = \frac{k_1 I_v(k_4 + k_5)[M]}{k_2(k_4 + k_5) + k_3 k_5[M]} \#(6)$$

And thus, by substituting back in Eq. (1)

$$\frac{d[M]}{dt} = \frac{-2k_1 I_v k_3 k_5[M]^2}{k_2(k_4 + k_5) + k_3 k_5[M]} = -2k_1 I_v \frac{[M]^2}{K + [M]} \#(7)$$

where $K = \frac{k_2(k_4 + k_5)}{k_3 k_5}$

The reaction appears of pseudo second order in $[M]$ for $[M] \ll K$. Instead for $[M] \gg K$ a pseudo first order is obtained, and this corresponds to a very small $k_2$ and/or a large $k_3$. Note that the addition of an excimer deactivation channel (either radiative or non-radiative) of the kind $MM^* \rightarrow M + M$, with

decay constant $k_6$, leaves unchanged the kinetic law of equation (7) but with the constants $k_1$ and $K$ replaced by more complex expressions.